Distributed Satellite Formation Based on Swarm Intelligence of Pigeon Flocks

1st Huaxin Qiu 2nd Qingrui Zhou* 3rd Changhao Sun 4th Xiaochu Wang 5th Yuting Feng

Qian Xuesen Laboratory of Space Technology
China Academy of Space Technology
Beijing, China
zhouqingrui@qxslab.cn

2020 Chinese Automation Congress (CAC) | 978-1-7281-7687-1/20/$31.00 ©2020 IEEE | DOI: 10.1109/CAC51589.2020.9326489

***Abstract*—In this paper, a collective motion model is established based on the mechanism of interaction pattern switching in pigeon flocks. Inspired by the swarm intelligence in the pigeon flocks, a distributed formation algorithm based on the model is proposed to coordinate a multi-satellite system to realize formation under environments with space debris and other obstacles. The comparative simulation with the traditional distributed algorithm without pattern switching is executed to verify the feasibility, validity, and superiority of the proposed algorithm.**

Keywords—collective motion, distributed control, satellite formation, swarm intelligence

I. INTRODUCTION

With the accelerative complexity of space tasks such as the scientific experiment, near-Earth survey, deep space exploration and interferometry, multiple small satellites are desperately anticipated to autonomously comprise a large or super-large virtual satellite or satellite network system by forming and retaining a given structure during on-orbit navigation [1]-[3].

In the homing flight of pigeons, Nagy et al. [4], [5] discovered a hierarchical network by recording the flight of 10 pigeons. Based on the data, Zhang et al. [6], [7] discovered that the pigeon flock adopts two interaction patterns alternately. When flying smoothly, pigeons will follow the average flight direction of their neighbors. When suddenly turning, they will follow their leaders. Although the qualitative analysis makes the pigeon swarm intelligence mechanism gradually limpid, it brings obstacles to reveal the simple rules behind the orderly movement of pigeon flocks due to the lack of clear description of interaction patterns and switching relationships. A collective motion model of pigeon flocks is built based on the multi-agent consensus control framework to describe the mechanism of interaction pattern switching [8]-[10].

In terms of the theoretical framework of multi-satellite distributed control and the application requirement of low-intelligence platform [11], [12], it is bitterly suitable to map bird swarm intelligence to autonomous coordination of multi-satellite formation. In this paper, the problem of satellite formation is transformed into the consensus problem of multi-satellites on the orbital normal plane in the reference orbit coordinate system with the help of Clohessy-Wiltshire (C-W) equations [13], [14]. Based on the collective motion model of pigeon flocks, a satellite distributed formation algorithm is proposed. Compared with traditional distributed algorithms without the interaction pattern switching, the proposed satellite distributed formation algorithm achieves better synchronization level and faster tracking speed with lower communication requirements.

The organization of the rest is as follows. Section II builds a collective motion model of pigeon flocks based on the mechanism of interaction pattern switching. Section III describes the satellite formation model. Section IV proposes a distributed formation algorithm for a multi-satellite system based on the models in Sections II and III. Simulations are described in Section V, and conclusions are given in Section VI.

II. COLLECTIVE MOTION MODEL OF PIGEON FLOCKS

By considering N pigeons within D -dimensional European space, each pigeon could be treated as a particle , and the following equation express its dynamics:

$$\begin{cases} \dot{\boldsymbol{x}}_i = \boldsymbol{v}_i \\ \dot{\boldsymbol{v}}_i = \boldsymbol{u}_i \end{cases} \tag{1}$$

where the index of pigeon $i = 1,...,N$, and $\boldsymbol{x}_i, \boldsymbol{v}_i, \boldsymbol{u}_i \in \mathrm{R}^{D\times 1}$ are the position vector, velocity vector and control input vector of pigeon i , respectively.

The following equation depicts the probability p_{h} that the pigeon flock adopts the hierarchical interaction pattern:

$$p_{\mathrm{h}} = \frac{1}{1+\alpha e^{-\beta \bar{K}^t}} \tag{2}$$

where $\alpha > 1$ and $\beta > 0$ are the parameters of the logistic function.

Supposing that the sampling time is t_{s} , the following

This work was supported in part by the China Postdoctoral Science Foundation under Grant 2020M670410 and the National Natural Science Foundation of China under Grant 61833009.

equation represents the neighbor set $\mathcal{N}_i^1$ in the egalitarian interaction pattern at the sample time point t_k:

$$\mathcal{N}_i^1(t_k)= \begin{cases} \left\{ j \middle| \left\| \boldsymbol{x}_{ij} \right\| \le R_{\mathrm{c}}^1 - R_{\mathrm{L}}^1, j \ne i \right\}, k = 0 \\ \left\{ j \middle| \begin{array}{l} \left\| \boldsymbol{x}_{ij} \right\| \le R_{\mathrm{c}}^1, j \in \mathcal{N}_i^1(t_{k-1}), j \ne i \quad \text{or} \\ \left\| \boldsymbol{x}_{ij} \right\| \le R_{\mathrm{c}}^1 - R_{\mathrm{L}}^1, j \notin \mathcal{N}_i^1(t_{k-1}), j \ne i \end{array} \right\}, k = 1,2,... \end{cases} \tag{3}$$

where $j = 1,...,N$, $\boldsymbol{x}_{ij} = \boldsymbol{x}_i - \boldsymbol{x}_j$ is the position vector of pigeon i relative to pigeon j, R_{c}^1 is the maximum communication distance in the egalitarian interaction pattern, and $R_{\mathrm{L}}^1 \in \left(0, R_{\mathrm{c}}^1\right)$ is the delay distance of adding connections between pigeons.

The following equation shows the neighbor set $\mathcal{N}_i^2$ in the hierarchical interaction pattern:

$$\mathcal{N}_i^2 = \left\{ j \middle| \left\| \boldsymbol{x}_{ij} \right\| \le R_{\mathrm{c}}^2, j \ne i, j = 1,...,N \right\} \tag{4}$$

where $R_{\mathrm{c}}^2 \ge R_{\mathrm{c}}^1$ is the maximum communication distance in the hierarchical interaction pattern.

Based on the above, each pigeon will calculate $\boldsymbol{u}_i$ based on neighbor interaction information and target location information to synchronize with neighbors, maintain the desired distance R_{d} with neighbors, and reach the target position vector $\boldsymbol{x}_{\mathrm{T}}$ with the maximum allowable error R_{L}^2:

$$\boldsymbol{u}_i = \begin{cases} -K^{\mathrm{F}} \sum\limits_{j \in \mathcal{N}_i^1} \nabla_{\boldsymbol{x}_i} V_{ij}^{\mathrm{F}} \left(\left\| \boldsymbol{x}_{ij} \right\| \right) \\ -K^{\mathrm{T}} \nabla_{\boldsymbol{x}_i} V_i^{\mathrm{T}} \left(\left\| \boldsymbol{x}_i - \boldsymbol{x}_{\mathrm{T}} \right\| \right) - K^{\mathrm{V}} w \sum\limits_{j \in \mathcal{N}_i} \boldsymbol{v}_{ij}, & i \in S_{\mathrm{d}} \\ -K^{\mathrm{F}} \sum\limits_{j \in \mathcal{N}_i^1} \nabla_{\boldsymbol{x}_i} V_{ij}^{\mathrm{F}} \left(\left\| \boldsymbol{x}_{ij} \right\| \right) \\ -K^{\mathrm{V}} \left(\sum\limits_{j \in \mathcal{N}_i \setminus S_{\mathrm{d}}} \boldsymbol{v}_{ij} + w \sum\limits_{j \in \mathcal{N}_i \cap S_{\mathrm{d}}} \boldsymbol{v}_{ij} \right), & i \notin S_{\mathrm{d}} \end{cases} \tag{5}$$

where S_{d} is the set of dominant pigeons with the location information of target T, $K^{\mathrm{F}} > 0$, $K^{\mathrm{T}} > 0$ and $K^{\mathrm{V}} > 0$ are the formation control gain, target control gain and alignment control gain respectively, and $\boldsymbol{v}_{ij} = \boldsymbol{v}_i - \boldsymbol{v}_j$ is the velocity vector of pigeon i relative to pigeon j. When the pigeon flock adopts the egalitarian interaction pattern, the current neighbor set $\mathcal{N}_i = \mathcal{N}_i^1$ and the alignment weight $w=1$; otherwise, $\mathcal{N}_i = \mathcal{N}_i^2$ and $w=w'$ where $w' \ge 1$ is the alignment weight in the hierarchical interaction pattern. The potential field function V_{ij}^{F} for formation is defined as follows:

$$V_{ij}^{\mathrm{F}} \left(\left\| \boldsymbol{x}_{ij} \right\| \right) = \begin{cases} \infty, & \text{if } \left\| \boldsymbol{x}_{ij} \right\| < R_{\mathrm{L}}^3 \\ \dfrac{1}{2} \left(\dfrac{R_{\mathrm{d}} \left(\left\| \boldsymbol{x}_{ij} \right\| - R_{\mathrm{L}}^3 \right)}{R_{\mathrm{d}} - R_{\mathrm{L}}^3} \right)^2 - \left(R_{\mathrm{d}} \right)^2 \mathrm{Ln} \dfrac{R_{\mathrm{d}} \left(\left\| \boldsymbol{x}_{ij} \right\| - R_{\mathrm{L}}^3 \right)}{R_{\mathrm{d}} - R_{\mathrm{L}}^3}, & \text{if } R_{\mathrm{L}}^3 \le \left\| \boldsymbol{x}_{ij} \right\| \le R_{\mathrm{d}} \\ \dfrac{1}{2} \left(\dfrac{R_{\mathrm{d}} \left(R_{\mathrm{c}}^1 - \left\| \boldsymbol{x}_{ij} \right\| \right)}{R_{\mathrm{c}}^1 - R_{\mathrm{d}}} \right)^2 - \left(R_{\mathrm{d}} \right)^2 \mathrm{Ln} \dfrac{R_{\mathrm{d}} \left(R_{\mathrm{c}}^1 - \left\| \boldsymbol{x}_{ij} \right\| \right)}{R_{\mathrm{c}}^1 - R_{\mathrm{d}}}, & \text{if } R_{\mathrm{d}} < \left\| \boldsymbol{x}_{ij} \right\| \le R \end{cases} \tag{6}$$

where R_{L}^3 is the minimum allowable distance between pigeons. The potential field function V_i^{T} of the target is defined as follows:

$$V_i^{\mathrm{T}} \left(\left\| \boldsymbol{x}_i - \boldsymbol{x}_{\mathrm{T}} \right\| \right) = \begin{cases} \dfrac{\left(\left\| \boldsymbol{x}_i - \boldsymbol{x}_{\mathrm{T}} \right\| - R_{\mathrm{L}}^2 \right)^3}{3}, & \left\| \boldsymbol{x}_i - \boldsymbol{x}_{\mathrm{T}} \right\| \ge R_{\mathrm{L}}^2 \\ 0, & 0 \le \left\| \boldsymbol{x}_i - \boldsymbol{x}_{\mathrm{T}} \right\| < R_{\mathrm{L}}^2 \end{cases} \tag{7}$$

III. Satellite Formation Model

Assuming that a target T is in a circular orbit, the position vector $\boldsymbol{P}_{\mathrm{T}} = \left[X_{\mathrm{T}}^{\mathrm{s}}, Y_{\mathrm{T}}^{\mathrm{s}}, Z_{\mathrm{T}}^{\mathrm{s}} \right]^{\mathrm{T}}$ of T in the Earth-Centered Inertial (ECI) coordinate system $\mathrm{O^sX^sY^sZ^s}$ is shown as follows:

$$\begin{bmatrix} X_{\mathrm{T}}^{\mathrm{s}} \\ Y_{\mathrm{T}}^{\mathrm{s}} \\ Z_{\mathrm{T}}^{\mathrm{s}} \end{bmatrix} = \mathbf{R}_{\mathbf{z}} \ \Omega_{\mathrm{T}} \ \mathbf{R}_{\mathbf{x}} \ i_{\mathrm{T}} \begin{bmatrix} r_{\mathrm{T}} \cos\theta_{\mathrm{T}} \\ r_{\mathrm{T}} \sin\theta_{\mathrm{T}} \\ 0 \end{bmatrix} \tag{8}$$

where Ω_{T}, i_{T} and r_{T} is the right ascension of the ascending node, orbital inclination and orbit radius of T respectively, $\theta_{\mathrm{T}} = \theta_{\mathrm{T}}^0 + n_{\mathrm{T}} t$ is the true anomaly of T, θ_{T}^0 is the initial true anomaly of T, $n_{\mathrm{T}} = \sqrt{r_{\mathrm{T}}^3 / \mu}$ is the orbital rate of T, $\mu = 398600.44 \mathrm{km}^3/\mathrm{s}^2$ is the geocentric gravitational constant, and the rotation matrices are as follows:

$$\mathbf{R}_{\mathbf{z}}\ \theta=\begin{bmatrix}\cos\theta & -\sin\theta & 0\\ \sin\theta & \cos\theta & 0\\ 0 & 0 & 1\end{bmatrix} \tag{9}$$

$$\mathbf{R}_{\mathbf{x}}\ \theta=\begin{bmatrix}1 & 0 & 0\\ 0 & \cos\theta & -\sin\theta\\ 0 & \sin\theta & \cos\theta\end{bmatrix} \tag{10}$$

The relative motion of satellite i relative to T could be expressed by the C-W equations [13], [14]:

$$\begin{cases}\ddot{x}_i^{\mathrm{s}}-2n_{\mathrm{T}}\dot{y}_i^{\mathrm{s}}-3{n_{\mathrm{T}}}^2x_i^{\mathrm{s}}=f_i^{\mathrm{x}}\\ \ddot{y}_i^{\mathrm{s}}+2n_{\mathrm{T}}\dot{x}_i^{\mathrm{s}}=f_i^{\mathrm{y}}\\ \ddot{z}_i^{\mathrm{s}}+{n_{\mathrm{T}}}^2z_i^{\mathrm{s}}=f_i^{\mathrm{z}}\end{cases} \tag{11}$$

where $x_i^{\mathrm{s}},y_i^{\mathrm{s}},z_i^{\mathrm{s}}$ is the position of i in the reference orbital coordinate system $\mathrm{o^sx^sy^sz^s}$ of T, and f_i^{x}, f_i^{y} and f_i^{z} are the acceleration component produced by the control force on the $\mathrm{x^s}$-axis, $\mathrm{y^s}$-axis and $\mathrm{z^s}$-axis, respectively. The origin $\mathrm{o^s}$ is located in the position of T, the $\mathrm{x^s}$-axis is along $\boldsymbol{P}_{\mathrm{T}}$, the $\mathrm{z^s}$-axis is along the angular momentum vector of T, and the $\mathrm{y^s}$-axis completes the right-handed system. It should be noted that since this paper focuses more on the guidance control of satellite formation, more accurate dynamic model is not considered.

The position vector $\boldsymbol{P}_i=\left[X_i^{\mathrm{s}},Y_i^{\mathrm{s}},Z_i^{\mathrm{s}}\right]^{\mathrm{T}}$ of i in the $\mathrm{O^sX^sY^sZ^s}$ is shown as follows:

$$\begin{bmatrix}X_i^{\mathrm{s}}\\ Y_i^{\mathrm{s}}\\ Z_i^{\mathrm{s}}\end{bmatrix}=\mathbf{R}_{\mathbf{z}}\ \Omega_{\mathrm{T}}\ \mathbf{R}_{\mathbf{x}}\ i_{\mathrm{T}}\ \mathbf{R}_{\mathbf{z}}\ \theta_{\mathrm{T}}\begin{bmatrix}x_i^{\mathrm{s}}\\ y_i^{\mathrm{s}}\\ z_i^{\mathrm{s}}\end{bmatrix}+\boldsymbol{P}_{\mathrm{T}} \tag{12}$$

IV. Satellite Formation Based on Pigeon Collective Motion Model

For achieving autonomous formation of a multi-satellite system, a distributed algorithm is proposed by mapping the model in Section II to the satellite formation control. As shown in Fig. 1, the satellite formation control is decoupled into the control on the $\mathrm{o^sy^sz^s}$ plane and the control in the direction of the $\mathrm{x^s}$-axis. On the $\mathrm{o^sy^sz^s}$ plane, each satellite not only conducts formation, alignment and target tracking based on the model in Section III but also evades obstacles. In the direction of the $\mathrm{x^s}$-axis, each satellite attempts to remain on the $\mathrm{o^sy^sz^s}$ plane. To improve formation synchronization, the probability p_{h} that each satellite adopts the hierarchical interaction pattern is related to the order parameter V_{a} rather than the curvature:

$$p_{\mathrm{h}}=\frac{1}{1+\alpha e^{-\beta(1-V_{\mathrm{a}})}} \tag{13}$$

where $V_{\mathrm{a}}=\left|\sum_{i=1}^{N}\boldsymbol{v}_i^*\right|/N$ is applied to measure the synchronization of satellites. It should be noted that due to the limitations of information acquisition in the distributed framework, the actual order parameters adopted by satellites is $V_{\mathrm{a}}=\left|\sum_{j\in\mathcal{N}_i\cup i}\boldsymbol{v}_j^*\right|/\left(\left|\mathcal{N}_i\right|+1\right)$ where $|A|$ is the number of elements in set A. The detailed algorithm is described as follows.

Step 1: Regard the current coordinates $\left[z_i^{\mathrm{s}},y_i^{\mathrm{s}}\right]^{\mathrm{T}}$ of satellite i as the position vector $\boldsymbol{x}_i$ of pigeon i. Set the current position vector $\boldsymbol{x}_{\mathrm{T}}$ of the target T as $[0,0]^{\mathrm{T}}$. Set the current position vector $\boldsymbol{x}_j^{\mathrm{O}}$ of obstacle j as $\left[z_j^{\mathrm{O}},y_j^{\mathrm{O}}\right]^{\mathrm{T}}$, where $j=1,\ldots,N_{\mathrm{O}}$, N_{O} is the number of obstacles, and y_j^{O} and z_j^{O} are the current position component of the center of j in $\mathrm{y^s}$-axis and $\mathrm{z^s}$-axis, respectively.

Step 2: Calculate the interaction pattern based on the probability p_{h}. The corresponding current neighbor set $\mathcal{N}_i$ and alignment weight w of satellite i are produced based on the pattern.

Step 3: Calculate current control input vector $\boldsymbol{u}_i$ of satellite i by the following equation:

$$\boldsymbol{u}_i=\begin{cases}-K^{\mathrm{f}}\sum\limits_{j\in\mathcal{N}_i^1}\nabla_{\boldsymbol{x}_i}V_{ij}^{\mathrm{F}}\left(\left\|\boldsymbol{x}_{ij}\right\|\right)\\ -K^{\mathrm{O}}\sum\limits_{j=1}^{N_{\mathrm{O}}}\nabla_{\boldsymbol{x}_i}V_i^{\mathrm{O}}\left(\left\|\boldsymbol{x}_i-\boldsymbol{x}_j^{\mathrm{O}}\right\|\right) & i\in S_{\mathrm{d}}\\ -K^{\mathrm{T}}\nabla_{\boldsymbol{x}_i}V_i^{\mathrm{T}}\left(\left\|\boldsymbol{x}_i-\boldsymbol{x}_{\mathrm{T}}\right\|\right)-K^{\mathrm{V}}w\sum\limits_{j\in\mathcal{N}_i}\boldsymbol{v}_{ij},\\ -K^{\mathrm{f}}\sum\limits_{j\in\mathcal{N}_i^1}\nabla_{\boldsymbol{x}_i}V_{ij}^{\mathrm{F}}\left(\left\|\boldsymbol{x}_{ij}\right\|\right)\\ -K^{\mathrm{O}}\sum\limits_{j=1}^{N_{\mathrm{O}}}\nabla_{\boldsymbol{x}_i}V_i^{\mathrm{O}}\left(\left\|\boldsymbol{x}_i-\boldsymbol{x}_j^{\mathrm{O}}\right\|\right) & i\notin S_{\mathrm{d}}\\ -K^{\mathrm{V}}\left(\sum\limits_{j\in\mathcal{N}_i\setminus S_{\mathrm{d}}}\boldsymbol{v}_{ij}+w\sum\limits_{j\in\mathcal{N}_i\cap S_{\mathrm{d}}}\boldsymbol{v}_{ij}\right),\end{cases} \tag{14}$$

where $K^{\mathrm{O}}>0$ is the obstacle avoidance gain, and the potential field function for obstacles is defined as follows:

$$V_i^{\mathrm{O}}\left(\left\|\boldsymbol{x}_i-\boldsymbol{x}_j^{\mathrm{O}}\right\|\right)=$$

$$\begin{cases} \infty, & \text{if } \left\|\boldsymbol{x}_i-\boldsymbol{x}_j^{\mathrm{O}}\right\| < r_j^{\mathrm{O}}+R_{\mathrm{L}}^4 \\ \dfrac{1}{2}\left(\dfrac{\left(r_j^{\mathrm{O}}+R_{\mathrm{c}}^3\right)\cdot\left(\left\|\boldsymbol{x}_i-\boldsymbol{x}_j^{\mathrm{O}}\right\|-r_j^{\mathrm{O}}-R_{\mathrm{L}}^4\right)}{R_{\mathrm{c}}^3-R_{\mathrm{L}}^4}\right)^2- & \text{if } r_j^{\mathrm{O}}+R_{\mathrm{L}}^4 \le \left\|\boldsymbol{x}_i-\boldsymbol{x}_j^{\mathrm{O}}\right\| \le \left(r_j^{\mathrm{O}}+R_{\mathrm{c}}^3\right)\cdot \\ \quad \mathrm{Ln}\dfrac{\left(\left\|\boldsymbol{x}_i-\boldsymbol{x}_j^{\mathrm{O}}\right\|-r_j^{\mathrm{O}}-R_{\mathrm{L}}^4\right)}{R_{\mathrm{c}}^3-R_{\mathrm{L}}^4}, & \le r_j^{\mathrm{O}}+R_{\mathrm{c}}^3 \\ \dfrac{1}{2}\left(r_j^{\mathrm{O}}+R_{\mathrm{c}}^3\right)^2- & \text{if } r_j^{\mathrm{O}}+R_{\mathrm{c}}^3 < \left\|\boldsymbol{x}_i-\boldsymbol{x}_j^{\mathrm{O}}\right\| \\ \quad \left(r_j^{\mathrm{O}}+R_{\mathrm{c}}^3\right)^2\mathrm{Ln}\left(r_j^{\mathrm{O}}+R_{\mathrm{c}}^3\right), & \end{cases} \tag{15}$$

where r_j^{O} is the radius of obstacle j, R_{c}^3 is the maximum detected distance of obstacles, and R_{L}^4 is the minimum allowable distance between satellites and obstacles.

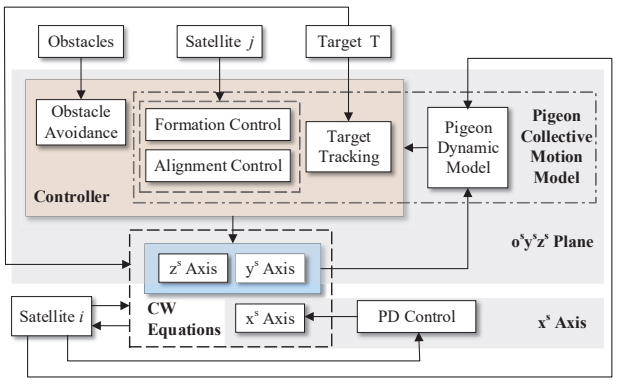

Fig. 1. Satellite formation frame based on pigeon collective motion model.

Step 4: Generate current $\ddot{x}_i^{\mathrm{s}}$ by the following equation [15]:

$$\ddot{x}_i^{\mathrm{s}}=-K^{\mathrm{P}}x_i^{\mathrm{s}}-K^{\mathrm{D}}\dot{x}_i^{\mathrm{s}} \tag{16}$$

where $K^{\mathrm{P}}>0$ and $K^{\mathrm{D}}>0$ are the proportion control gain and differential control gain in the x^{s}-axis direction.

Step 5: Produce the acceleration component $\left(f_i^{\mathrm{x}},f_i^{\mathrm{y}},f_i^{\mathrm{z}}\right)$ by (11) where $\ddot{z}_i^{\mathrm{s}}=\boldsymbol{u}_i^1$ and $\ddot{y}_i^{\mathrm{s}}=\boldsymbol{u}_i^2$. Modify current control input vector $\boldsymbol{u}_i$ by the following equations:

$$\boldsymbol{u}_i^1=\begin{cases} f_{\max}^z-{n_{\mathrm{T}}}^2z_i^{\mathrm{s}}, & \text{if } f_i^{\mathrm{z}}>f_{\max}^z \\ \boldsymbol{u}_i^1, & \text{if } f_{\min}^z\le f_i^{\mathrm{z}}\le f_{\max}^z \\ f_{\min}^z-{n_{\mathrm{T}}}^2z_i^{\mathrm{s}}, & \text{if } f_i^{\mathrm{z}}<f_{\min}^z \end{cases} \tag{17}$$

$$\boldsymbol{u}_i^2=\begin{cases} f_{\max}^{\mathrm{y}}-{n_{\mathrm{T}}}^2z_i^{\mathrm{s}} & \text{if } f_i^{\mathrm{y}}>f_{\max}^{\mathrm{y}} \\ \boldsymbol{u}_i^2, & \text{if } f_{\min}^{\mathrm{y}}\le f_i^{\mathrm{y}}\le f_{\max}^{\mathrm{y}} \\ f_{\min}^{\mathrm{y}}-{n_{\mathrm{T}}}^2z_i^{\mathrm{s}}, & \text{if } f_i^{\mathrm{y}}<f_{\min}^{\mathrm{y}} \end{cases} \tag{18}$$

where $f_{\max}^{\mathrm{y}}$ and $f_{\max}^z$ are the upper limit of the acceleration component on the y^{s}-axis and z^{s}-axis respectively, and $f_{\min}^{\mathrm{y}}$ and $f_{\min}^z$ are the corresponding lower limit.

Modify current $\ddot{x}_i^{\mathrm{s}}$ by the following equation:

$$\ddot{x}_i^{\mathrm{s}}=\begin{cases} f_{\max}^{\mathrm{x}}+2n_{\mathrm{T}}\dot{y}_i^{\mathrm{s}}+3{n_{\mathrm{T}}}^2x_i^{\mathrm{s}}, & \text{if } f_i^{\mathrm{x}}>f_{\max}^{\mathrm{x}} \\ \ddot{x}_i^{\mathrm{s}}, & \text{if } f_{\min}^{\mathrm{x}}\le f_i^{\mathrm{x}}\le f_{\max}^{\mathrm{x}} \\ f_{\min}^{\mathrm{x}}+2n_{\mathrm{T}}\dot{y}_i^{\mathrm{s}}+3{n_{\mathrm{T}}}^2x_i^{\mathrm{s}}, & \text{if } f_i^{\mathrm{x}}<f_{\min}^{\mathrm{x}} \end{cases} \tag{19}$$

where $f_{\max}^{\mathrm{x}}$ and $f_{\min}^{\mathrm{x}}$ are the upper limit and lower limit of the acceleration component on the x^{s}-axis, respectively.

Step 6: Gain the position vector $\boldsymbol{x}_i$ at the next time by (1). Set $\left[z_i^{\mathrm{s}},y_i^{\mathrm{s}}\right]^{\mathrm{T}}$ as $\boldsymbol{x}_i$.

Step 7: Obtain the position vectors of the target and satellites by (8) and (12), respectively.

V. Simulation Results

To verify the feasibility and effectiveness of the proposed algorithm in Section V, 10 satellites are assigned to track a target in formation under the environment with space debris or other obstacles.

The parameters of the target are set as follows: $\Omega_{\mathrm{T}}=\pi/6$, $i_{\mathrm{T}}=\pi/4$, $r_{\mathrm{T}}=7400000\mathrm{m}$ and $\theta_{\mathrm{T}}^0=0$. The parameters of obstacles are set as follows: $\left[z_1^{\mathrm{O}},y_1^{\mathrm{O}}\right]=-400\mathrm{m},-80\mathrm{m}$, $r_1^{\mathrm{O}}=100\mathrm{m}$; $\left[z_2^{\mathrm{O}},y_2^{\mathrm{O}}\right]=-800\mathrm{m},130\mathrm{m}$, $r_2^{\mathrm{O}}=80\mathrm{m}$. The initial state of satellites in $\mathrm{o^s x^s y^s z^s}$ coordinate system is shown in Table I. The acceleration limit of satellites are as follows: $f_{\max}^{\mathrm{x}}=f_{\max}^{\mathrm{y}}=f_{\max}^z=5\mathrm{m/s^2}$ and $f_{\min}^{\mathrm{x}}=f_{\min}^{\mathrm{y}}=f_{\min}^z=-5\mathrm{m/s^2}$. The maximum communication distance of satellites is 150m. The minimum allowable distance between satellites is 20m. The multi-satellite system is required to track the target with an allowable error of 50m in formation and to maintain a distance of not less than 10m from obstacles. The maximum detected distance of obstacles is 100m.

Each satellite controls itself autonomously according to **Algorithm 1**. The parameters of **Algorithm 1** are set as

follows: T_{max}=6000s , t_s=0.1s , N=10 , D=2 , α=150 , β=8.2 , $S_d=\{4,8\}$, R_c^1=135m , R_c^2=150m , R_c^3=100m , R_d=50m , R_L^1=1m , R_L^2=5m, R_c^3=10m, R_L^4=10m , R_L^3=20m , K^F=0.45 , K^V=1.6 , K^T=0.1 , K^O=5 , K^P=0.2 , K^D=0.2 , w'=6.5 , and V_{max}=20m/s .

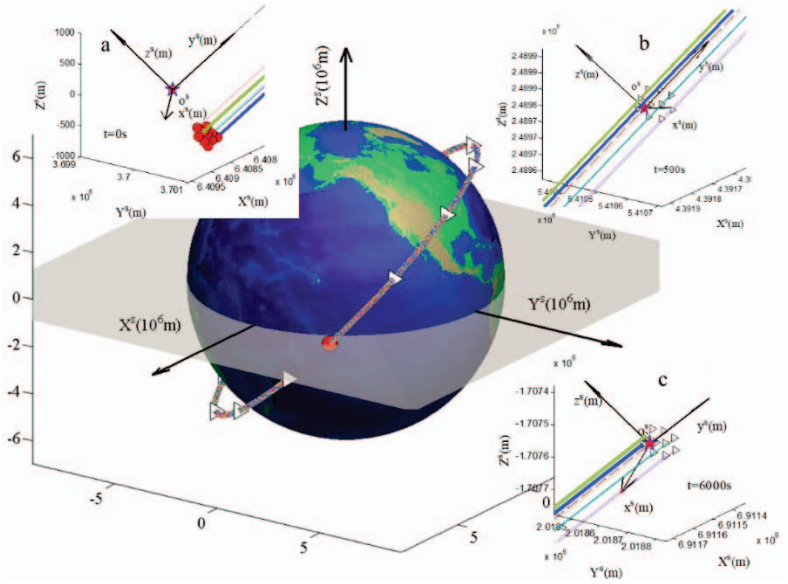

Fig. 2. Satellite formation in the ECI coordinate system.

TABLE I. INITIAL STATE OF SATELLITES

i	x_i^s m	y_i^s m	z_i^s m	$\dot{x}_i^s$ m/s	$\dot{y}_i^s$ m/s	$\dot{z}_i^s$ m/s
1	0.6	-163.0	-694.4	-2.3	1.0	-3.0
2	-1.6	-45.1	-783.6	0.2	3.5	1.5
3	-4.5	-139.7	-807.3	4.6	0.5	4.3
4	1.0	-242.8	-806	-1.4	2.2	0.2
5	0.7	-64.8	-918.5	-4.8	4.2	-4.9
6	-0.5	-145.6	-894.9	3.2	4.2	-1.7
7	3.0	-244.7	-926.7	-1.3	-1.1	-3.5
8	4.2	-49.0	-1007.1	-2.6	-4.5	-4.6
9	3.8	-139.7	-990.3	3.3	-4.6	-2.5
10	-4.9	-250.7	-1011.5	-1.5	2.0	-4.0

Fig. 2 depicts the satellite formation trajectory in the ECI coordinate system. In Fig. 2, the initial positions of satellites are marked with solid circles, and the positions are marked with solid triangles every 500s. As shown in Fig. 2, the multi-satellite system could navigate around the earth as a whole without clustering based on **Algorithm 1**. The insets a-b in Fig. 2 are the enlarged snapshots of the satellite formation trajectories at 0s, 500s and 6000s, respectively. In the insets, the target T , the origin o^s of the $o^sx^sy^sz^s$ coordinate system, is marked with a pentagon. The trajectory of T is marked with a dotted line. The trajectories of dominant satellites and ordinary satellites are marked with heavy lines and thin lines, respectively. As shown in the insets, the multi-satellite system could track the target in formation before $t = 500$s , and keep formation in subsequent flight.

Fig. 3 displays the satellite formation trajectory in the reference orbital coordinate system before the allowable error of target tracking is satisfied, where Fig. 3(a) and Fig. 3(b) describe the trajectory in the $o^sx^sy^sz^s$ coordinate system and the $o^sy^sz^s$ plane, respectively. In Fig. 3, the target T is marked with a pentagon. Obstacles are marked with cylinders, and the areas with the minimum allowable distance from the obstacles are marked by the surfaces outside the cylinders. The initial positions and final positions of satellites are marked with solid circles and solid triangles, respectively. The trajectories of dominant satellites and ordinary satellites are marked with heavy solid lines and thin dotted lines, respectively. As shown in Fig. 3(a), the multi-satellite system could gradually converge to the same plane and reach the target in formation. As shown in Fig. 3(b), the multi-satellite system could safely navigate under the obstacle environment.

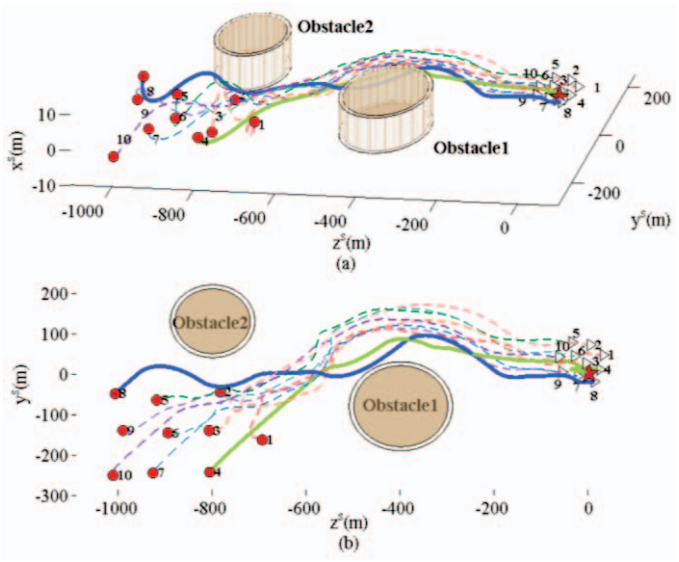

Fig. 3. Satellite formation in the reference orbital coordinate system. (a) In the $o^sx^sy^sz^s$ coordinate system. (b) On the $o^sy^sz^s$ plane.

In order to further verify the superiority of **Algorithm 1**, the comparative simulation based on the traditional distributed method is also carried out. Considering that there is no interactive pattern switching in traditional methods, each satellite is set to adopt only the egalitarian interaction pattern (i.e. $\alpha=\infty$ and $\beta<\infty$ to make $p_{\mathrm{h}}=0$) in the contrast simulation. Considering the fairness and effectiveness of comparisons, the initial conditions and other parameters of the simulation without pattern switching are the same as those of the above simulation except that R_{c}^{1}=150m . Fig. 4 shows the comparative result with and without interaction pattern switching, where Fig. 4(a)-(c) describe the order parameter, the average distance between satellites, and the average distance between a satellite and the target, respectively. In Fig. 4, the results with and without interaction pattern switching are marked with heavy solid lines and heavy dotted lines, respectively. As shown in Fig. 4(a), the multi-satellite system with switching could achieve a higher level of synchronization faster than a non-switch system, and the final synchronization of the switch system is better than that of the non-switch system at the same time. Besides, the average synchronization of the switch system (as shown by the thin dotted line) is also better than that of the non-switch system (as shown by the thin dash-dotted line) during the same period. As shown in Fig. 4(b), the average distance between satellites in the switch system tends to be stable at about 58s, which is 2s faster than that of non-switch systems. As shown in Fig. 4(c), the average distance between the target and a satellite in the switch system is less than the allowable error of target tracking (as shown by the thin dash-dotted line) at about 61s, whereas the tracking error of the non-switch system fails to meet the requirement at this time.

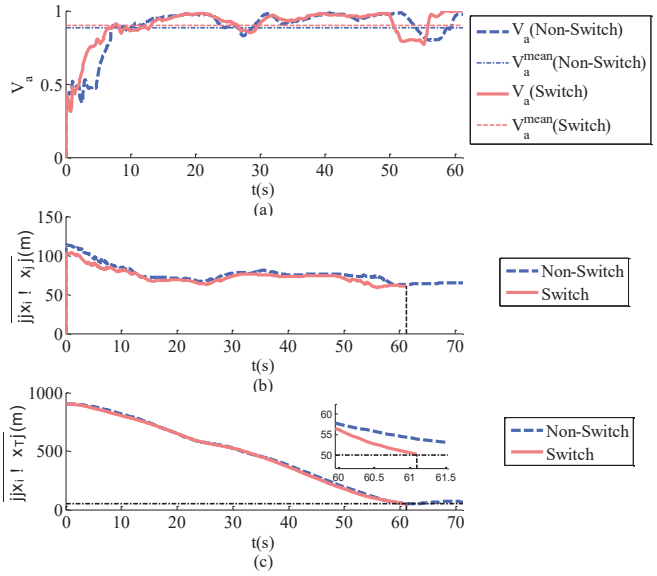

Fig. 4. Comparison between switch and non-switch. (a) Order parameter. (b) Average distance between satellites. (c) Average distance between a satellite and the target.

In summary, a multi-satellite system based on **Algorithm 1** could track a target in formation under the environment with space debris or other obstacles. Compared with systems without interactive pattern switching, the switch system based on **Algorithm 1** has advantages in the synchronization, formation stability and tracking rapidity.

VI. Conclusion

This paper presented a distributed satellite formation algorithm inspired by the swarm intelligence of pigeon flocks. Compared with the centralized algorithm, the proposed algorithm possess superior scalability and reliability by supporting satellite online joining or exiting. Compared with the traditional distributed algorithm without pattern switching, the proposed algorithm has smaller communication loads and computing requirements by the interaction pattern switching. In the future, we will focus on the improvement of the distributed algorithm and the validation on the physical simulation system of satellite formation.

References

[1] B. S. Yu, Z. Huang, L. L. Geng, and D. P. Jin, "Stability and ground experiments of a spinning triangular tethered satellite formation on a low earth orbit," *Aerosp. Sci. Technol.*, vol. 92, pp. 595-604, Sep. 2019.

[2] K. S. El Maghraby, A. Grubišić, C. Colombo, and A. Tatnall, "A novel interferometric microwave radiometer concept using satellite formation flight for geostationary atmospheric sounding," *IEEE T. Geosci. Remote.*, vol. 56, no. 6, pp. 3487-3498, Jun. 2018.

[3] L. Cao, Y. Chen, Z. Zhang, H. Li, and A. K. Misra, "Predictive smooth variable structure filter for attitude synchronization estimation during satellite formation flying," *IEEE T. Aero. Elec. Sys.*, vol. 53, no. 3, pp. 1375-1383, Jun. 2017.

[4] M. Nagy, Z. Ákos, D. Biro, and T. Vicsek, "Hierarchical group dynamics in pigeon flocks," *Nature*, vol. 464, no. 7290, pp. 890-893, Apr. 2010.

[5] M. Nagy, G. Vásárhelyi, B. Pettit, I. Roberts-Mariani, T. Vicsek, and D. Biroa, "Context-dependent hierarchies in pigeons," *P. Natl. Acad. Sci.*, vol. 110, no. 32, pp. 13049-13054, Aug. 2013.

[6] H. T. Zhang, Z. Y. Chen, T. Vicsek, G. Feng, L. Sun, R. Su, and T. Zhou "Route-dependent switch between hierarchical and egalitarian strategies in pigeon flocks," *Sci. Rep.*, vol. 4, p. 5805, Jul. 2014.

[7] D. Chen, T. Vicsek, X. Liu, T. Zhou, and H. T. Zhang, "Switching hierarchical leadership mechanism in homing flight of pigeon flocks," *Europhys. Lett.*, Vol. 114, No. 6, p. 60008, Jul. 2016.

[8] Y. Tang, Z. Deng, and Y. Hong, "Optimal output consensus of high-order multiagent systems with embedded technique," *IEEE Trans. Cybern.*, vol. 49, no. 5, pp. 1768-1779, May 2019.

[9] X. Dong, and G. Hu, "Time-varying formation tracking for linear multiagent systems with multiple leaders," *IEEE T. Automat. Contr.*, vol. 62, no. 7, Jul. 2017.

[10] Z. Cheng, H. T. Zhang, M. C. Fan, and G. Chen, "Distributed consensus of multi-agent systems with input constraints: a model predictive control approach," *IEEE T. Circuits-I*, vol. 62, no. 3, pp. 825-834, Mar. 2015.

[11] C. Sun, W. Sun, X. Wang, and Q. Zhou, "Potential game theoretic learning for the minimal weighted vertex cover in distributed networking systems," *IEEE Trans. Cybern.*, vol. 49, no. 5, pp. 1968-1978, May 2019.

[12] H. Qiu, and H. Duan, "Multiple UAV distributed close formation control based on in-flight leadership hierarchies of pigeon flocks," *Aerosp. Sci. Technol.*, Vol. 70, pp. 471-486, Nov. 2017.

[13] B. Zhou, and J. Lam, "Global stabilization of linearized spacecraft rendezvous system by saturated linear feedback," *IEEE T. Contr. Syst. T.*, vol. 25, no. 6, pp. 2185-2193, Jan. 2017.

[14] C. Peng, and Y. Gao, "Formation-flying planar periodic orbits in the presence of intersatellite Lorentz force," *IEEE T. Aero. Elec. Sys.*, vol. 53, no. 3, pp. 1412-1430, Jun. 2017.

[15] H. Qiu, and H. Duan, "A multi-objective pigeon-inspired optimization approach to UAV distributed flocking among obstacles," *Inform. Sciences*, vol. 509, pp. 515-529, Jan. 2020.